PCCP

PAPER

View Article Online
View Journal | View Issue

Cite this: *Phys. Chem. Chem. Phys.*, 2025, **27**, 17759

2,4,6-Triphenyl-1,3,5-triazine functionalized *fac*-tris(2-phenylpyridine)Ir(III) complexes with polarity sensitive T_1 state properties†

Peter I. Djurovich, Kelly K. Biv, Ruben Mirzoyan and Mark E. Thompson *

Received 18th March 2025,
Accepted 21st July 2025

DOI: 10.1039/d5cp01062d

rsc.li/pccp

Here, we report the synthesis and study of three Ir(III) complexes, which are derivatives of *fac*-Ir(ppy)$_3$ (Hppy – 2-phenylpyridine). In these derivatives, the third position of the pyridine ring of one of the ppy ligands is functionalized with a tolyl (**Ir-tol**) or triphenyl triazine group (**Ir-*meta*** and **Ir-*para***). **Ir-*meta*** has a 3-(3,5-diphenyl-2,4,6-triazinyl)phenyl group on the ppy pyridyl ligand, giving a *meta* disposition of the triazine to the ppy ligand, and **Ir-*para*** has a 4-(3,5-diphenyl-2,4,6-triazinyl)phenyl group bound to the ppy ligand, placing the triazine moiety *para* to the ppy ligand. The complex **Ir-tol** shows electrochemical properties and phosphorescence characteristics nearly identical to the unfunctionalized *fac*-Ir(ppy)$_3$. Complexes **Ir-*meta*** and **Ir-*para*** show reduction potentials that are anodically shifted from those of **Ir-tol** by *ca.* 0.6 V, consistent with the reduction centered on the triazine moiety. In non-polar media, the lowest triplet state (T_1) of **Ir-*meta*** and **Ir-*para*** has mixed metal-to-ligand charge transfer (MLCT) and ligand centered (LC) character localized on the Ir-ppy moiety of the functionalized ligand. With an increase in solvent polarity, *i.e.* CH_2Cl_2 and dimethyl sulfoxide (DMSO), the T_1 state of these complexes gains character of intraligand charge transfer (ILCT) from Ir-ppy to the triazine moiety of the functionalized ligand. This change in excited state character is accompanied by a distortion in the molecular geometry towards planarization of the acceptor and donor units. Such polarity-controlled modulation of T_1 state character is observed using transient absorption (TA) spectroscopy and is found to markedly affect the photoluminescence properties of the complexes.

Introduction

The photophysical properties of the complex of Ir(III) ions with three cyclometalated 2-phenylpyridine (**ppy**) ligands in a *facial* configuration (*fac*-Ir(ppy)$_3$: **Ir-ppy**), first reported by Watts and co-workers,[1] have been thoroughly investigated, due in large part to its high phosphorescence efficiency and comparatively short triplet lifetime.[2–9] These properties arise due to the role of the d^6 iridium(III) cation in the electronic structure of the complex, leading to several highest occupied molecular orbitals (HOMOs) of the complex possessing significant iridium 5d-orbital character. Hence, with several lowest unoccupied MOs (LUMOs) representing π* orbitals on the **ppy** ligands, the lowest excited states of **Ir-ppy** show significant metal-to-ligand charge transfer (MLCT) character. Spin multiplicity of the excited states is strongly affected by spin–orbit coupling (SOC) induced by the iridium center (ζ = 3909 cm^{-1}),[10] which activates the otherwise spin-forbidden intersystem crossing (ISC) and phosphorescence. Indeed, ISC ($S_1 \rightarrow T_1$) of **Ir-ppy** is fast with a time constant of $\tau_{ISC} \approx 100$ fs.[4] The $T_1 \rightarrow S_0$ phosphorescence of **Ir-ppy** is intense and characterized with a decay time constant of τ = 1.5–2 μs,[7,9] which is widely regarded as a benchmark value among mononuclear Ir(III) complexes, with only a few faster monometallic phosphorescing complexes.[11,12] Efficient population of the lowest triplet state and efficient phosphorescence have opened numerous applications for **Ir-ppy** and analogous organometallic iridium complexes, for instance, application in organic light emitting diodes,[3,13–17] cellular imaging[18–21] and photodynamic therapy,[22–24] photo-redox catalysis[25–27] and sensing.[20,22,28] The properties of these Ir-based materials are heavily influenced by the choice of the coordinated ligands.[27,29,30] One way to modulate photophysical properties is based on the localization of the triplet state in a heteroleptic complex, such that excitation can involve different ligands, but the excited molecule relaxes into the excited state involving the lowest energy ligand or the MLCT state.[31–36] Homoleptic complexes like **Ir-ppy** also tend to have their excited states localized on a single ligand, due to small energy

Department of Chemistry, University of Southern California, Los Angeles, California 90089, USA. E-mail: met@usc.edu

† Electronic supplementary information (ESI) available: Synthetic details and characterization of the complexes, and additional electrothermal data and photophysical data. See DOI: https://doi.org/10.1039/d5cp01062d

differences between the otherwise identical ligands in the relaxed triplet state.[37,38] In most heteroleptic complexes, the ligands that make up the complex are quite dissimilar, such that the energy difference between MLCT or mixed ligand-MLCT states involving the different ligands is substantially different; however, the nature of the excitation is quite similar. Here we present a set of derivatives of **Ir-ppy**, in which one of the ppy ligands is functionalized with a 2,4,6-triphenyl-1,3,5-triazine acceptor. In these heteroleptic complexes, the triplet excited state could be either MLCT, similar to the one that involves the other ppy ligands, or an intraligand charge transfer (ICT) transition, involving the triazine-ppy ligand. The strong SOC of the Ir(III) center is maintained in the lowest excited states. Control of the character of the T_1 state, namely, the extent of charge transfer to the triazine acceptor, is controlled *via* the medium polarity which markedly affects the energy of the ICT state.

Results and discussion

Synthesis

Ir(III) complexes were synthesized using a multistep process, starting from a dichloro-bridged dimer [*i.e.* $(ppy)_2Ir(\mu\text{-}Cl)_2Ir(ppy)_2$],[39] which reacted with 3-bromo-2-phenylpyridine in a 2-methoxyethanol : water mixture (4 : 1) in the presence of silver triflate to afford the tris-cyclometalated complex **Ir-Br** (Scheme 1). As reported by Dedeian *et al.*,[8] the reaction conditions utilized in the synthesis of **Ir-Br** (including water as a protic and coordinating solvent) afford the thermodynamically favored *facial* (*fac*) configuration of the ligands, rather than the *meridional* (*mer*) isomer. Notably, Watts and co-authors also mentioned a facile formation of the *fac*-isomer of **Ir-ppy** when the H-ppy ligand precursor reacts with the hydrated form of $IrCl_3$.[1] The final products (**Ir-tol**, **Ir-*meta*** and **Ir-*para***) were obtained *via* Suzuki coupling (Scheme 1).[40] These complexes are assigned as *fac*-isomers owing to their high photoluminescence efficiencies in toluene solution (*vide infra*), a property not characteristic of *mer*-isomers, which show efficient nonradiative decay due to photo-isomerization.[5,41] While all three complexes are soluble in toluene and dichloromethane, the **Ir-*meta*** and **Ir-*para*** complexes, especially the latter, are much less soluble in dimethyl sulfoxide (DMSO). It is also noteworthy that the ^{1}H NMR spectra of **Ir-tol** and **Ir-*para*** in DMSO-d_6 display broadened resonances for the pendant phenylene group indicative of slow dynamic exchange of the phenylenes caused by rotation around the bond linked to the pyridyl ligand (Fig. S2 and S4, ESI†).

Electrochemical analysis

Cyclic voltammetry (CV) and differential pulse voltammetry (DPV) electrochemical measurements were conducted for **Ir-tol**, **Ir-*meta*** and **Ir-*para*** in anhydrous *N*,*N*-dimethylformamide (DMF), using an internal ferrocenium/ferrocene couple as the reference potential. The obtained voltammograms and DPV curves are shown in Fig. S5 (ESI†), and pertinent data are collected in Table S1 (ESI†). The first oxidation and reduction waves of **Ir-tol** appear at E_{ox} = 0.33 V and E_{red} = −2.65 V. These values are close to those reported for **Ir-ppy** under the same conditions (E_{ox} = 0.31 V and E_{red} = −2.7 V).[5,8] In the case of **Ir-*meta*** the first oxidation and reduction potentials appear at E_{ox} = 0.31 V and E_{red} = −2.05 V, respectively. The oxidation potential is close to the value reported for **Ir-ppy**, whereas the reduction potential shows a significant anodic shift. The data suggest a similar make-up for the HOMOs of **Ir-*meta***, and **Ir-ppy**, but very different LUMOs. The reduction of **Ir-*meta*** likely takes place at the triazine moiety. Indeed, the CV and DPV measurements for 2,4,6-triphenyl-1,3,5-triazine give a reduction potential of −2.07 V under the same conditions (see Fig. S5, ESI†). Hence, we conclude that the LUMO of **Ir-*meta*** is localized on the 2,4,6-triphenyl-1,3,5-triazine unit. In the case of **Ir-*para***, the first oxidation and reduction reactions occur at E_{ox} = 0.35 V and E_{red} = −2.00 V, respectively. These potentials are anodically shifted by *ca.* 0.05 V compared to those measured for **Ir-*meta***, indicative of a slightly stronger electronic influence of the 1,3,5-triazine unit in **Ir-*para***.

Steady-state spectroscopy

Optical spectroscopic measurements of **Ir-tol**, **Ir-*meta*** and **Ir-*para*** were conducted in three different solvents: toluene, dichloromethane and dimethyl sulfoxide (DMSO) at a concentration of $\approx 10^{-5}$ M. The steady-state absorption and emission spectra are shown in Fig. 1, and pertinent data of photoluminescence characteristics are given in Table 1. The UV-visible absorption spectra of all three complexes in toluene are reminiscent of those of **Ir-ppy**[7,9] (see Fig. S6, ESI†). The low energy bands display features with moderate intensity (ε_{max} = 1.5 × 10^4 M^{-1} cm^{-1}) bearing relatively strong metal-to-ligand charge transfer (MLCT, d → π*) character admixed with ligand centered (LC, π → π*) transitions.[42] The absorption spectra of the

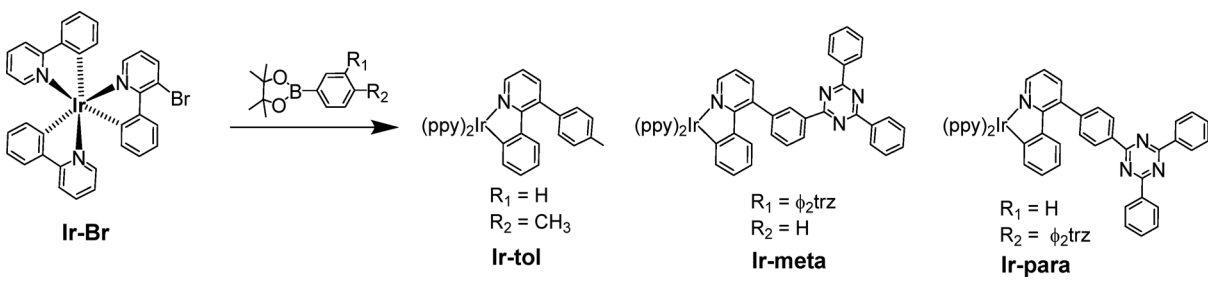

Scheme 1 Synthetic route to **Ir-tol**, **Ir-*meta*** and **Ir-*para***, $\phi_2$trz = 3,5-diphenyltriazine.

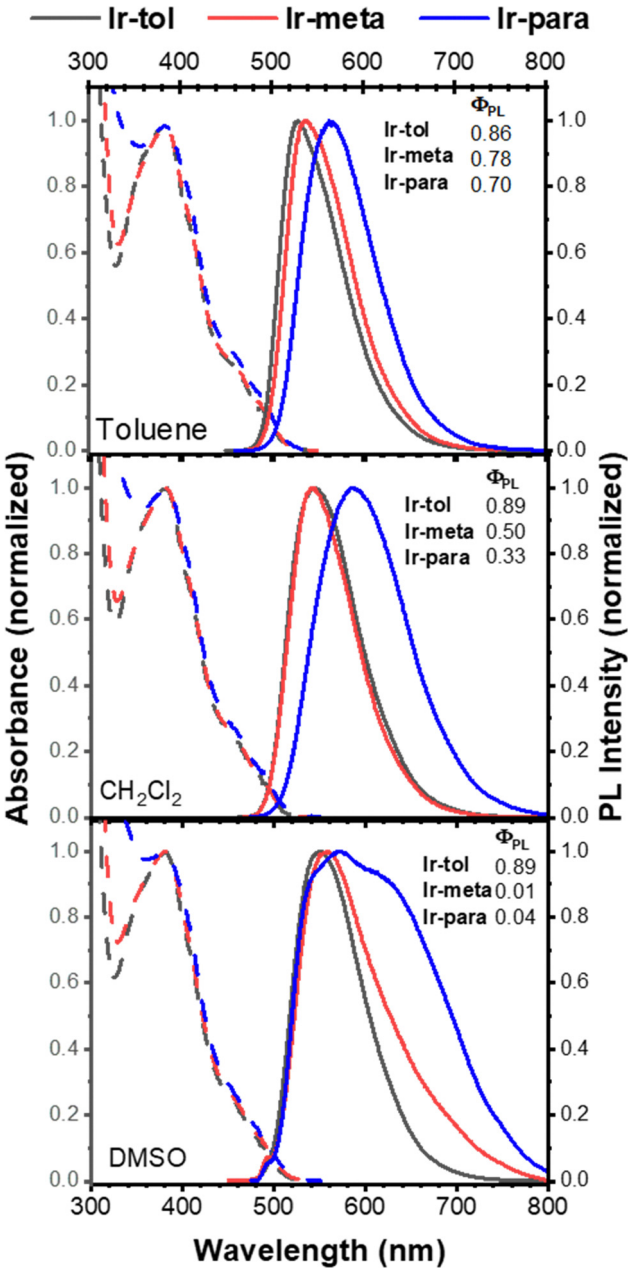

Fig. 1 Absorption (dashed) and emission (solid) spectra of **Ir-tol** (black), **Ir-*meta*** (red) and **Ir-*para*** (blue) at room temperature in toluene, CH_2Cl_2 and DMSO. Photoluminescence (PL) spectra were recorded in deoxygenated solvents. All samples were excited at 380 nm.

three Ir-based complexes are weakly perturbed regardless of the solvent polarity and thus nearly indistinguishable for all solutions (Fig. 1).

The photoluminescence spectrum of **Ir-tol** in toluene peaks at 529 nm, with an efficiency of Φ_{PL} = 0.86 and a decay time of τ = 1.47 μs at room temperature in deoxygenated solution (Table 1). The emission is effectively quenched by O_2 when the sample is exposed to the air (Φ_{PL} = 0.02 and τ = 35 ns). The emission efficiency and decay time constant for **Ir-tol** are similar to those for **Ir-ppy** under the same conditions[7] and

Table 1 A summary of the key photophysical properties of complexes **Ir-tol**, **Ir-*meta*** and **Ir-*para***. Emission was measured for dilute, deoxygenated solutions (≈10^{-5} M) at room temperature

Compound	Solvent	λ_{max}[a] (nm)	Φ_{PL}	τ[b] (μs)	k_r[c] (10^5 s^{-1})	k_{nr}[c] (10^5 s^{-1})
Ir-tol	Toluene	529	0.86	1.47	5.9	0.95
	CH_2Cl_2	544	0.89	1.67	5.3	0.65
	DMSO	549	0.89	1.51	5.3	0.73
Ir-*meta*	Toluene	536	0.78	1.48	5.3	1.5
	CH_2Cl_2	544	0.50	1.00	5.0	5.0
	DMSO	558	0.01	0.059 (93%)	—	—
				1.25 (7%)		
Ir-*para*	Toluene	563	0.70	2.20	3.2	1.4
	CH_2Cl_2	585	0.33	0.57	5.8	11.8
	DMSO	573	0.04	0.029 (89%)	—	—
		615(sh)		0.77 (11%)		

[a] Samples were excited at 380 nm. [b] Samples were excited at 405 nm (1 ns laser pulse) and were well fit with a single exponential decay unless listed otherwise. [c] The radiative rates are calculated as $k_r = \Phi_{PL}/\tau$; the non-radiative decay rates are calculated as $k_{nr} = (1 - \Phi_{PL})/\tau$.

consistent with $T_1 \rightarrow S_0$ phosphorescence having a lowest excited state with significant ^{3}MLCT character.[14,43] A red-shift in the emission maximum for **Ir-tol** compared to that for **Ir-ppy** (λ_{max} = 510 nm, see Fig. S6, ESI†) suggests that the emitting triplet state of **Ir-tol** is localized on the tolyl functionalized ppy ligand. The emission maximum of **Ir-tol** undergoes a bathochromic shift in polar CH_2Cl_2 (λ_{max} = 544 nm) and DMSO (λ_{max} = 549 nm). Nevertheless, the photoluminescence efficiency and decay time constants remain comparable to those in toluene (Φ_{PL} = 0.89 and τ = 1.67 μs in CH_2Cl_2 and Φ_{PL} = 0.89 and τ = 1.51 μs in DMSO).

The $T_1 \rightarrow S_0$ phosphorescence of **Ir-*meta*** in toluene solution (λ_{max} = 536 nm, Φ_{PL} = 0.78 and τ = 1.48 μs) is similar to that of **Ir-tol**. Apparently, the 2,4,6-triphenyl-1,3,5-triazine substituent of **Ir-*meta*** exerts a minimal effect on the energy and character of the emitting T_1 state in this solvent. However, in polar CH_2Cl_2, luminescence efficiency decreases (λ_{max} = 544 nm and Φ_{PL} = 50%) along with a decrease of the decay time constant (τ = 1.0 μs). The radiative decay rate (k_r) of **Ir-*meta*** is nearly constant in both solvents, so the decrease in emission efficiency in CH_2Cl_2 is primarily due to enhanced non-radiative decay (k_{nr}) (Table 1). In more polar DMSO, the spectrum peaks at 558 nm and broadens with the emission tail extending to lower energy (Fig. 1). The photoluminescence efficiency of **Ir-*meta*** also decreases precipitously (Φ_{PL} = 1%). The emission decay curve in DMSO (λ_{det} = 560 nm) is biexponential, with two components having distinct decay time constants (τ) and corresponding intensity fractions (f_i) (τ_1 = 59 ns, f_1 = 0.93 and τ_2 = 1.25 μs, f_2 = 0.07; Fig. 2).

The photophysical behavior of **Ir-*para*** is similar to that of **Ir-*meta***. Photoluminescence from **Ir-*para*** in toluene solution is intense and red-shifted (λ_{max} = 563 nm, Φ_{PL} = 70% and τ = 2.2 μs), consistent with emission having ^{3}MLCT character. In polar CH_2Cl_2, photoluminescence of **Ir-*para*** bathochromically shifts (λ_{max} = 585 nm) and the emission efficiency and decay time constant substantially decrease (Φ_{PL} = 33% and τ = 0.57 μs), a change principally due to an increase in the rate

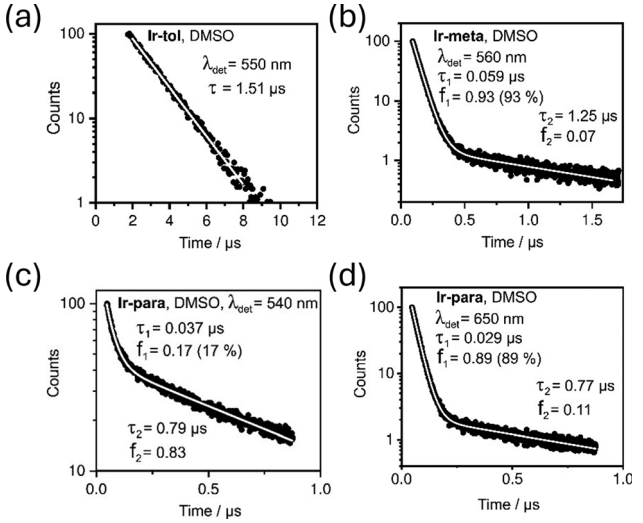

Fig. 2 Emission decay curves of deoxygenated DMSO solution samples excited at 405 nm (laser pulse = 1 ns) of (a) **Ir-tol**, (b) **Ir-*meta*** and (c) and (d) **Ir-*para***. The fractional intensities are found as $f_1 = \alpha_1\tau_1/(\alpha_1\tau_1 + \alpha_2\tau_2)$ and $f_2 = \alpha_2\tau_2/(\alpha_1\tau_1 + \alpha_2\tau_2)$, where α_1 and α_2 are amplitudes corresponding to τ_1 and τ_2, respectively.[44]

for non-radiative decay. In more polar DMSO, the photoluminescence spectrum of **Ir-*para*** displays a broad manifold (λ_{max} = 573 nm with shoulders at 540 and *ca.* 615 nm) that has a low efficiency (Φ_{PL} = 4%). The luminescence lineshape indicates the presence of at least two weakly emissive species, one at high energy corresponding to the ^{3}MLCT transition and another at lower energy. The emission decay curve measured at λ_{det} = 540 nm in DMSO has two components with distinct time constants and corresponding intensity fractions (τ_1 = 37 ns, f_1 = 0.17 and τ_2 = 0.79 μs with f_2 = 0.83) (Fig. 2). Detection at 650 nm gives similar decay constants with lower weighting for the long-lived component (τ_1 = 29 ns, f_1 = 0.89 and τ_2= 0.77 μs, f_2 = 0.11) (Fig. 2).

The luminescence properties of **Ir-*meta*** and **Ir-*para*** in polar media provide evidence for the presence of additional low energy excited states. The redox potentials for the complexes would place an ILCT state at *ca.* 2.36 eV (525 nm), an energy not far from that of the ^{3}MLCT state. Judged by the radiative decay times, the fast component in the excited state decays from **Ir-*meta*** and **Ir-*para*** can be assigned to a state with ^{3}MLCT character. This state non-radiatively decays in polar solvents to either a dark ILCT state or a ground state at a rate much higher than the ~1 μs radiative decay. Therefore, the nature of the slow decay component could be either due to ligand-based phosphorescence or thermal promotion to the bright ^{3}MLCT from the long-lived dark state.

Transient absorption spectroscopy and spectro-electrochemical studies

While the solvatochromic shift in emission energy between toluene, CH_2Cl_2 and DMSO is similar for the three complexes, the solvent dependence of the photoluminescence efficiency for **Ir-*meta*** and **Ir-*para*** differs markedly from that of **Ir-tol**.

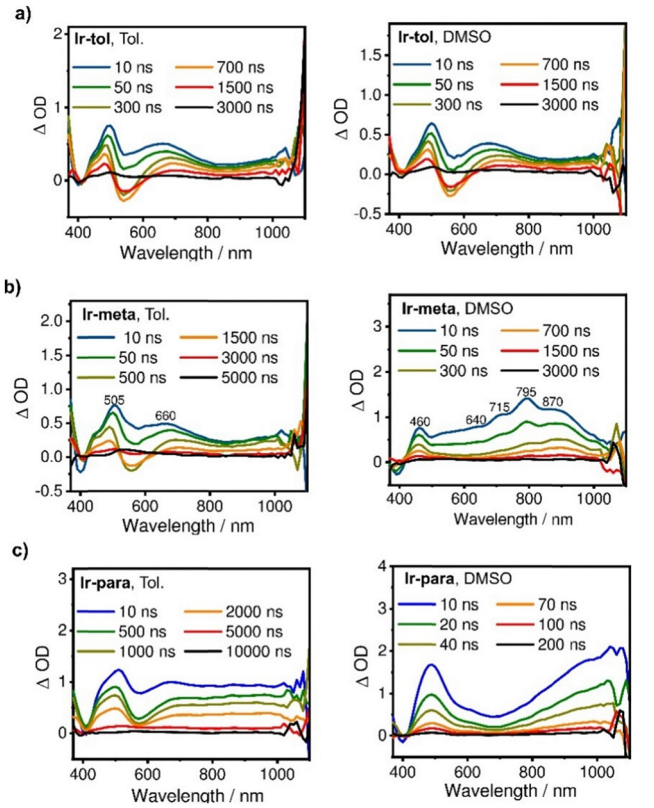

Fig. 3 TA spectra measured for (a) **Ir-tol**, (b) **Ir-*meta***, and (c) **Ir-*para*** in toluene (Tol.) and DMSO.

The triazine function strongly affects the non-radiative properties of the T_1 state in polar solvents, leading to a substantial decrease in Φ_{PL}. The Ir complexes were thus investigated using nanosecond transient absorption (TA) spectroscopy in polar and nonpolar solvents to probe the nature of these excited state properties. The TA experiments were conducted with deoxygenated solutions in a 10 ns to 10 μs time range using a pump wavelength of 355 nm (1 ns pulse) and a probe spanning the 370–1100 nm spectral window (Fig. 3). The TA data were collected for all three complexes in toluene, CH_2Cl_2 and DMSO. Partial decomposition was observed for the CH_2Cl_2 samples over the course of data collection, so the analysis presented here will focus only on the toluene and DMSO samples. The spectra recorded in CH_2Cl_2 are given in the ESI.†

The TA spectrum of **Ir-tol** at 10 ns measured in toluene shows a positive band at *ca.* 505 nm with a shoulder at *ca.* 445 nm and a broad band centered at *ca.* 660 nm (Fig. 3a). The spectral feature centered at *ca.* 540 nm appearing as a bleach at long time delays is assigned to incomplete subtraction of the emission signal of the complex, a problem that occurs with highly luminescent materials. The transient absorption of **Ir-*meta*** in toluene (Fig. 3b) appears and develops in a comparable manner to that of **Ir-tol**. Such a close similarity of the TA features of the two complexes in toluene substantiates that the nature of the T_1 state for **Ir-tol** and **Ir-*meta*** is the same in this medium and thus assigned to have mixed MLCT/LC character. In contrast, the TA spectra obtained for **Ir-*para*** in

toluene differ in that the feature associated with emission centered at *ca.* 570 nm develops relatively fast in the first 500 ns but does not cross the zero-line of the optical density axis (likely due to its lower Φ_{PL}) and shows a broad absorption signal in the range of 700–1000 nm (Fig. 3c). Evidently, the latter broad signal is related to both the presence of the triazine function in the molecule and its *para*-position with respect to the pyridine ring of the functionalized ligand.

The TA spectra of the three compounds in DMSO in Fig. 3 differ significantly from each other. The spectra of **Ir-tol** in DMSO remain similar to that measured in toluene, indicating that the character of the T_1 state is preserved despite the large increase in solvent polarity. In contrast, the TA spectra of **Ir-*meta*** in DMSO exhibit a positive band at *ca.* 460 nm and a band at *ca.* 795 nm, with shoulders at *ca.* 640 nm and 715 nm (Fig. 3b). The spectrum of **Ir-*para*** in DMSO appears distinct from that of **Ir-*meta*** and exhibits a positive band at *ca.* 500 nm and a broad band intensifying in the range of 800–1000 nm (Fig. 3c). The TA signals for the excited state of **Ir-*para*** also decay at a rate that is an order of magnitude faster than that of **Ir-*meta***. Such a marked difference in the TA spectra of the **Ir-*meta*** and **Ir-*para*** in DMSO, compared to the spectra obtained for toluene solutions, suggests that the T_1 state undergoes a significant change in character in polar media. The change could be associated with an increased contribution of charge transfer to the triphenyl-triazine acceptor to the T_1 state in polar media.

To explore the nature of the ILCT states, we carried out spectro-electrochemical measurements with 2,4,6-triphenyl-1,3,5-triazine under an applied reducing potential (Fig. 4). The spectra thus obtained display bands at 345 nm, 640 nm, 715 nm and *ca.* 800 nm upon reduction. The bands appearing at 640 nm, 715 nm and 800 nm for the anionic form of 2,4,6-triphenyl-1,3,5-triazine closely reproduce the bands at 640 nm, 715 nm and 795 nm observed in the TA spectra of **Ir-*meta*** in DMSO. Therefore, the strong contribution from the charge transfer state indicates that the T_1 states of the triazine functionalized Ir complexes are more stabilized in polar DMSO. It is noted that in the case of **Ir-*para***, the TA signals in DMSO do not reproduce the absorption signal of reduced 2,4,6-triphenyl-1,3,5-triazine as closely as observed for **Ir-*meta***. This difference is consistent with the triazine moiety being more isolated from the ppy ligand in **Ir-*meta*** than in **Ir-*para***. Conjugation to the pyridyl group of the ppy ligand in **Ir-*para*** leads to a less vibronic structure in the spectra of the reduced ligand (*vide supra*). The TA measurements collected using CH_2Cl_2 solutions suffered from relatively fast sample degradation but agree qualitatively with the plots measured in DMSO (see the ESI†).

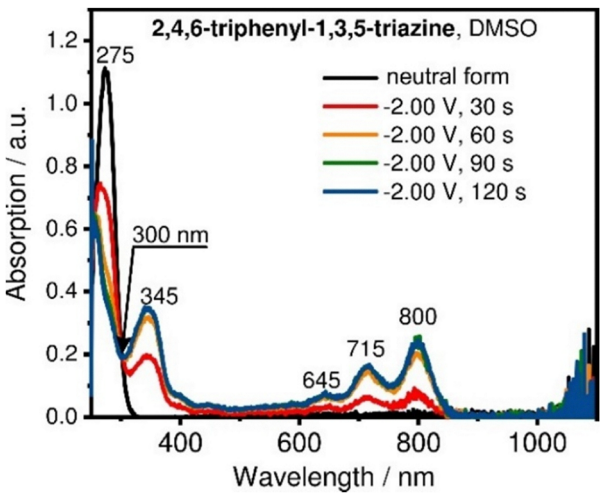

Fig. 4 Absorption spectra of 2,4,6-triphenyl-1,3,5-triazine, taken for the neutral form (black line) and upon reduction at −2 V *vs.* $Fc^{0/1+}$ wave after the indicated amount of time.

Since the overall emission quantum yields of **Ir-*meta*** and **Ir-*para*** in DMSO are low, the intensity for contributions of the two emission decay components obtained using time-correlated single photon counting (TCSPC) measurements do not represent real concentrations of their associated species. To address this point, we analyzed the decay of the TA signal at wavelength slices corresponding to bands appearing in DMSO (Fig. S8, ESI†). The wavelength measured at 800 nm for **Ir-*meta*** was fit using a two-exponential function, giving decay time constants of 59 ns and 530 ns. The shorter time constant reproduces the value obtained using TCSPC measured for the fast decay component of **Ir-*meta*** in DMSO (τ = 59 ns). The 1000 nm wavelength slice of TA data of **Ir-*para*** in DMSO is represented by a distinct mono-exponential component of TA signal decay with a time constant of 29 ns, which matches the time constant of the fast component of the TCSPC measured emission decay, discussed above.

These data correlate the TA absorption bands with the fast decay component of emission in DMSO, which we attribute to excited species with a MLCT dominant triplet state. With this being the case and the TA spectral features remaining unchanged throughout the experimental timeframe, we presume that the triplet state in polar solvents undergoes fast relaxation to a dark ILCT state with substantial triazine-based charge transfer character. The slow component of the TCSPC trace then comes from thermal promotion from the dark ILCT state to the bright MLCT state.

Computational analysis and discussion

To gain further understanding of the photophysical properties of the complexes from the standpoint of molecular electronic structure, quantum-chemical calculations were performed using the Q-Chem package.[45] Density functional theory (DFT) at the B3LYP[46]/LACVP[47] level was utilized with effective core potentials (ECPs) for the Ir atoms. Excited states were calculated using the random phase approximation (RPA) method.[48–50] We assume that the triplet state of either of the three complexes is populated by ultrafast intersystem crossing after photoexcitation, similar to that found for **Ir-ppy**.[51,52] Therefore, since we are interested in understanding the $T_1 \rightarrow S_0$ transition paths of these complexes, our discussion will primarily be focused on the T_1 state properties.

The complexes in the ground electronic state are found to have slightly twisted geometry of the functionalized ligand with

the dihedral angles between coordinated phenyl and pyridyl rings (ppy fragment) being 12° in **Ir-tol**, 7° in **Ir-*meta*** and 16° in **Ir-*para***, whereas dihedral angle in the unfunctionalized ppy ligands is *ca.* 1°. Also, in the functionalized ligand, the calculated dihedral angle between the coordinated pyridyl ring and the connected phenylene ring of triphenyltriazine, hereafter referred to as the θ-angle, varies in complexes **Ir-tol** (θ = 62°), **Ir-*meta*** (θ = 71°) and **Ir-*para*** (θ = 55°). These large dihedral angles are imposed by steric interactions with the nearby coordinated phenyl moiety of the ppy ligand.

The selected valence molecular orbitals of **Ir-tol**, **Ir-*meta*** and **Ir-*para*** in their ground state geometries are shown in Fig. 5. The HOMO in all three compounds has a common electronic structure comprising an Ir d_{z^2} orbital and three phenyl π orbitals. The LUMO, LUMO+1 and LUMO+2 in **Ir-tol** are composed of the π* orbital delocalized over the three cyclometalated phenyl-pyridine units. The negligible stabilization imparted by the *p*-tolyl substituent is likely a result of the relatively large dihedral angle between the arene and the pyridyl ligand. In both **Ir-*meta*** and **Ir-*para***, the LUMO and LUMO+1 represent π* orbitals on the triphenyltriazine moiety. These orbitals are near degenerate in **Ir-*meta*** as there is a node in the LUMO+1 at the carbon atom linking the *meta*-substituted phenylene group to the pyridyl ring, whereas the LUMO in **Ir-*para*** has bonding character between the carbon atoms linking the pyridyl ring with the *para*-substituted phenylene ring of the triphenyltriazine moiety. Thus, in contrast to **Ir-*meta***, the populated LUMO of **Ir-*para*** can conjugate the triazine acceptor with the cyclometalated phenylpyridyl unit of the functionalized ligand, leading to enhanced stabilization relative to LUMO+1. The LUMO+2 in both **Ir-*meta*** and **Ir-*para*** is similar in energy and orbital composition to the LUMO of **Ir-tol**. The computational results support the conclusion based on the electrochemical data of a minor perturbation of the cyclometalated ppy ligand by the triazine acceptor in **Ir-*meta*** and relatively stronger electronic influence in the case of **Ir-*para***.

The lowest triplet states of the complexes were investigated regarding their photoluminescent properties. Upon DFT geometry optimization, the T_1 state of **Ir-tol** in the gas phase finds a global minimum localized on the tolyl functionalized ligand with the $T_1 \rightarrow S_0$ vertical excitation energy of 2.47 eV (502 nm). The electronic spin density of the T_1 state for **Ir-tol** in the relaxed geometry demonstrates the mixed MLCT/LC character of the T_1 state (Fig. 6). The localization of the relaxed T_1 state on the functionalized ligand aligns with the rationale given above for the slight redshift of **Ir-tol** phosphorescence compared to that of **Ir-ppy**. The geometric distortions in the T_1 state are most reflected in shortening of the bond between the metalated phenyl and substituted pyridyl, as well as in the coordination bonds to the functionalized ligand (accommodating the excited state), and elongation of coordination bonds to the unfunctionalized ligands. Specifically, the calculated C_{Ph}–C_{pyr} bond length (1.42 Å) is 0.04 Å shorter than the corresponding bond lengths of the other ligands. Likewise, the Ir–C and Ir–N coordination bond lengths to the functionalized ligand in the relaxed T_1 state geometry are 1.99 Å and 2.13 Å, respectively,

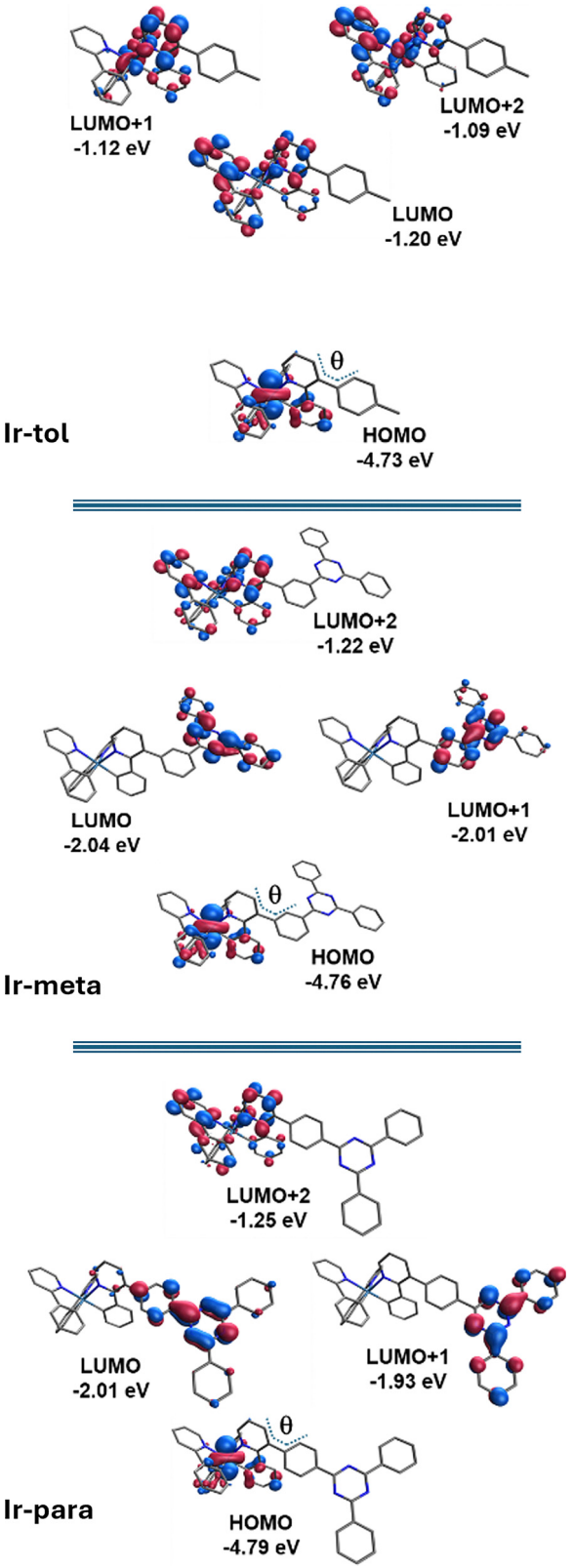

Fig. 5 Iso-surface contour plots (iso-value = 0.1) of valence molecular orbitals for **Ir-tol**, **Ir-*meta*** and **Ir-*para*** in ground state (S_0) optimized (DFT) geometries. The dihedral angle between the pyridyl and phenylene rings of the functionalized ligand is indicated by θ.

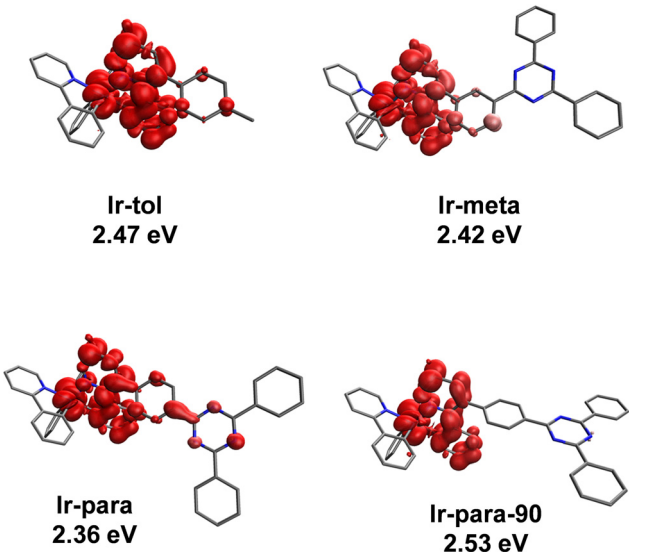

Fig. 6 Optimized geometries and iso-surface contour plots (iso-value = 0.02) of the spin density for the T_1 state. The values for the $T_1 \leftarrow S_0$ vertical excitation energy are given for each structure.

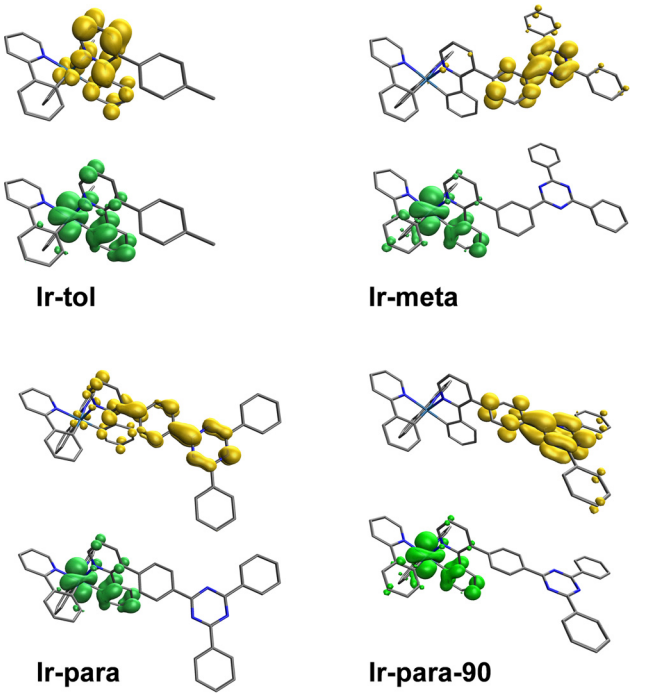

Fig. 7 Iso-surface contour plots (iso-value = 0.100) obtained for the NTOs of the T_1 state for the Ir complexes in their S_0 geometries. The hole is in green, and the electron is in yellow.

whereas the distances are 2.04 Å and 2.19 Å, respectively, to the unfunctionalized ligands. A similar geometric reorganization pattern upon localization of the T_1 state on a ligand was also calculated and discussed by Marian *et al.* for **Ir-ppy**.[38] Importantly, along with the changes in coordination bond lengths, the dihedral angle in the functionalized ligand decreased significantly (θ = 47°) in T_1 state geometry. The decrease in the dihedral angle allows spin density to extend onto the pendant *p*-tolyl ring. A corresponding localization on the substituted phenylpyridyl ligand occurs in the optimized T_1 geometry for **Ir-*meta*** and **Ir-*para*** where the dihedral angle decreased significantly in **Ir-*meta*** (θ = 44°) and **Ir-*para*** (θ = 39°) in T_1 state geometry. The $T_1 \rightarrow S_0$ vertical excitation energy for **Ir-*meta*** is 2.42 eV (513 nm), and for **Ir-*para***, it is 2.36 eV (525 nm). When the dihedral angle for **Ir-*para*** is constrained to 90° (**Ir-*para*-90**), the spin density no longer extends onto the pendant triphenyltriazine and the $T_1 \rightarrow S_0$ vertical excitation energy increases to 2.53 eV (489 nm).

The excited state properties of the complexes were further analyzed using TD-DFT calculations. The presence of local (MLCT) and long range (ILCT) (ppy-to-triazine) charge transfer transitions in **Ir-*meta*** and **Ir-*para*** made accurate modeling problematic, owing to the well-known difficulties for TD-DFT to account for CT transitions with a poor orbital overlap.[53] Standard TDDFT calculations provided consistent energies for the lowest MLCT transition (2.77 eV, 445 nm) for all three complexes; however, energies for the long range CT in **Ir-*meta*** and **Ir-*para*** were grossly underestimated, falling to 2.38 eV for the former and 2.43 eV for the latter complex. Application of coulomb attenuation methods (CAM) to the exchange increased the energy of the long-range CT state above that of the MLCT state. The energy of the lowest MLCT state also increased to around 3.10 eV for all the complexes. Nevertheless, the nature of the long-range CT in the T_1 state can be best understood using natural transition orbitals (NTOs) obtained using calculations without CAM exchange and is thus shown in Fig. 7.

The calculated electronic configuration for the T_1 state shows that the electron hole is localized on the Ir atom and the metalated phenyl of the substituted ligand in all the complexes. The electron is localized on the phenylpyridyl ligand in **Ir-tol**, whereas the position shifts onto the phenyltriazine moiety in the other derivatives. There is minimal electron density on the pyridyl ring in **Ir-*meta***, whereas **Ir-*para*** has a noticeably larger contribution from the phenylpyridyl ligand. Electron density is absent on the phenylpyridyl ligand upon rotation of the phenylene group in **Ir-*para*-90**. The poor overlap between the hole and the electron in the CT state for **Ir-*meta*** effectively separates the charges onto the metal–ligand and the phenyltriazine. This decoupled electronic configuration will suppress the rate of charge separation and radiative decay as well as promote non-radiative deactivation of the excited state. A similar situation is present in **Ir-*para***; however, the extent to which the hole and the electron are coupled will vary depending on the dihedral angle between the phenylene and pyridyl ligand. The acute angle in **Ir-*para*** allows for enhanced conjugation between the phenyltriazine and phenylpyridyl ligand, whereas the orthogonal orientation in **Ir-*para*-90** leads to slow—but complete—charge separation analogous to that found in **Ir-*meta***.

Calculations were carried out for the anionic forms of **Ir-*meta*** and **Ir-*para*** to account for the difference in the TA spectra observed in these complexes in DMSO (Fig. 8). The spin density derived from these calculations can be used to evaluate the extent of electron localization in the long-range CT state. The dihedral angle in **Ir-*meta*** (θ = 70°) remains close to the value in

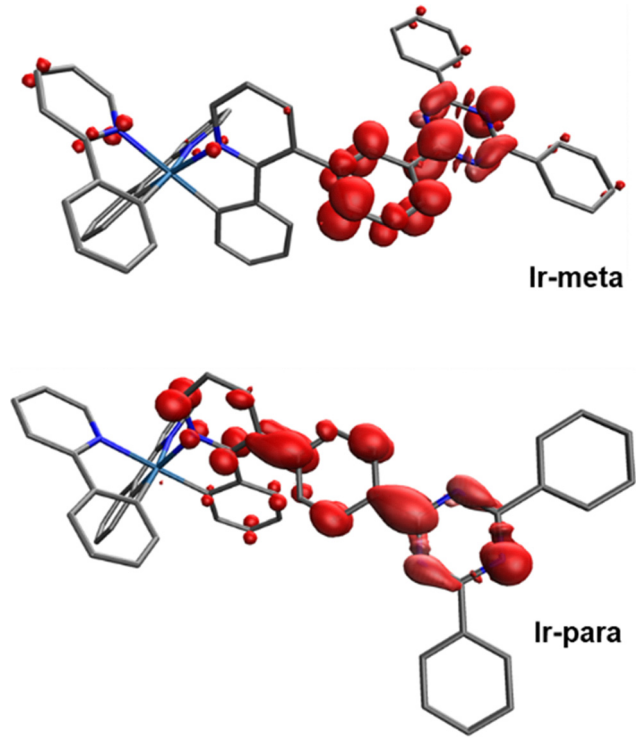

Fig. 8 Iso-surface contour plots (iso-value = 0.02) of the spin density for the anionic structures of **Ir-*meta*** and **Ir-*para***.

the neutral S_0 state; however, the value in **Ir-*para*** (θ = 40°) decreased significantly in the anionic geometry. The charge localization in **Ir-*meta*** is similar to that calculated for triphenyltriazine, whereas charge localization in **Ir-*para*** extends onto the pyridyl ligand. Therefore, the increase in delocalization for **Ir-*para*** likely is responsible for the bathochromic shift in the positive near-infrared band observed for the excited state in the TA spectra.

Summary

We demonstrate a synthetic approach to tailoring transition metal complexes *via* on-complex ligand functionalization. In this work, the approach afforded novel complexes **Ir-tol**, **Ir-*meta*** and **Ir-*para*** and a simple method of introducing a triphenyl triazine acceptor group at a sterically encumbered position of a cyclometalated ligand is demonstrated using well-established cross-coupling protocols. The photoluminescence properties of **Ir-tol** are reminiscent of the unfunctionalized **Ir-ppy** with efficient phosphorescence stemming from the MLCT/LC character T_1 state under both non-polar toluene and polar DMSO solution conditions. The T_1 state character and photoluminescence properties of both acceptor functionalized complexes **Ir-*meta*** and **Ir-*para*** are sensitive to increased solvent polarity manifested by a marked decrease of phosphorescence efficiency. Analysis of electronic structures of the three complexes by computational methods, conducted with an eye on the TA data, suggests that the structurally relaxed T_1 state localizes primarily on the cyclometalated Ir-ppy part of the functionalized ligand. With an increase in medium polarity, electron density in the T_1 state of **Ir-*meta*** and **Ir-*para*** extends onto the triphenyltriazine group and gains ILCT character, affording a larger dipole moment and additional stabilization due to the solvation energy. Extension of the T_1 state localization onto the acceptor is concurrent with distortion of molecular geometry towards planarization of the functionalized ligand, which is more favorable in the case of **Ir-*para***. The increasing involvement of the triazine acceptor in the T_1 state with the increase of solvent polarity is also manifested in the evolution of the nanosecond TA spectra where new red-shifted positive bands appear in DMSO solution. Indeed, conjugation of the pyridyl and phenylene rings in the T_1 state of **Ir-*para*** in DMSO results in more red shifted TA bands (800–1000 nm), whereas for **Ir-*meta***, the TA bands appearing in DMSO solution (640–800 nm) are more reminiscent of the absorption spectrum of reduced 2,4,6-triphenyl-1,3,5-triazine. Finally, the ILCT nature of the T_1 state for **Ir-*meta*** and **Ir-*para*** accounts for the decrease in phosphorescence efficiency in polar solvents. In polar solvents, the ILCT red shifts to fall lower in energy than the MLCT state, and thus the emission involves thermal promotion from the weakly emissive or dark ILCT state to the bright MLCT state.

Experimental

The detailed syntheses of **Ir-tol**, **Ir-*meta***, and **Ir-*para*** and their characterization are given in the ESI.† Electrochemical and photophysical measurements were carried out using anhydrous Supelco solvents. NMR spectra were taken with a Varian 400 MHz (^{1}H) instrument. UV-visible absorption spectra were taken with an Agilent 4853 diode array spectrophotometer. Photoluminescence quantum yields were measured using a Hamamatsu C9920 integrating sphere system. Emission lifetimes were obtained using time correlated single photon counting (TCSPC). Emission lifetime and quantum yield measurements were conducted for samples deoxygenated by purging nitrogen gas through the sample solution. Steady-state emission spectra were obtained with a QuantaMaster model C-60SE spectrofluorometer of Photon Technology International. Transient absorption experiments were conducted with a Magnitude Envision instrument. Cyclic voltammetry and differential pulse voltammetry measurements were conducted using an EG&G Model 283 potentiostat/galvanostat with 0.1 M tetra-*n*-butylammonium hexafluorophosphate in *N*,*N*-dimethylformamide as an electrolyte under a nitrogen atmosphere. The working, counter, and pseudo-reference electrodes were composed of glassy carbon, platinum wire, and silver wire, respectively. The ferrocene redox couple was used as the internal references for all electrochemical measurements.

Conflicts of interest

One of the authors, Thompson, has a financial interest in the Universal Display Corporation (UDC), one of the funding sources for this work.

Data availability

The data supporting this article have been included as part of the ESI.†

Acknowledgements

The authors would like to thank Dr Marsel Z. Shafikov for his contributions to this work. He prepared the complexes, carried out much of the photophysical and electrochemical measurements and generated early drafts of the manuscript. We are disappointed that he chose to not be a coauthor of this study. The authors would like to acknowledge the Department of Energy, Office of Energy Efficiency and Renewable Energy, Award: EE0009688 (Shafikov, Biv), and the Universal Display Corporation (Djurovich, Thompson) for support. Funds were provided by the National Science Foundation (award: CHE-2018740) to acquire the X-ray diffractometer that was used to determine the crystal structures reported here. In addition, we thank the National Science Foundation (CHE-0840366) for the funds to acquire the NMR spectrometer used in our work.

References

1 K. A. King, P. J. Spellane and R. J. Watts, Excited-State Properties of a Triply Ortho-Metalated iridium(III) Complex, *J. Am. Chem. Soc.*, 1985, **107**(5), 1431–1432, DOI: **10.1021/ja00291a064**.

2 K. Dedeian, P. I. Djurovich, F. O. Garces, G. Carlson and R. J. Watts, A New Synthetic Route to the Preparation of a Series of Strong Photoreducing Agents: Fac-Tris-Ortho-Metalated Complexes of Iridium(III) with Substituted 2-Phenylpyridines, *Inorg. Chem.*, 1991, **30**(8), 1685–1687, DOI: **10.1021/ic00008a003**.

3 M. A. Baldo, S. Lamansky, P. E. Burrows, M. E. Thompson and S. R. Forrest, Very High-Efficiency Green Organic Light-Emitting Devices Based on Electrophosphorescence, *Appl. Phys. Lett.*, 1999, **75**(1), 4–6, DOI: **10.1063/1.124258**.

4 K.-C. Tang, K. L. Liu and I. C. Chen, Rapid Intersystem Crossing in Highly Phosphorescent Iridium Complexes, *Chem. Phys. Lett.*, 2004, **386**(4–6), 437–441, DOI: **10.1016/j.cplett.2004.01.098**.

5 A. B. Tamayo, B. D. Alleyne, P. I. Djurovich, S. Lamansky, I. Tsyba, N. N. Ho, R. Bau and M. E. Thompson, Synthesis and Characterization of Facial and Meridional Tris-Cyclometalated Iridium(III) Complexes, *J. Am. Chem. Soc.*, 2003, **125**(24), 7377–7387, DOI: **10.1021/ja034537z**.

6 W. J. Finkenzeller and H. Yersin, Emission of $Ir(Ppy)_3$. Temperature Dependence, Decay Dynamics, and Magnetic Field Properties, *Chem. Phys. Lett.*, 2003, **377**(3–4), 299–305, DOI: **10.1016/S0009-2614(03)01142-4**.

7 W. Holzer, A. Penzkofer and T. Tsuboi, Absorption and Emission Spectroscopic Characterization of $Ir(Ppy)_3$, *Chem. Phys.*, 2005, **308**(1), 93–102, DOI: **10.1016/j.chemphys.2004.07.051**.

8 K. Dedeian, J. Shi, N. Shepherd, E. Forsythe and D. C. Morton, Photophysical and Electrochemical Properties of Heteroleptic Tris-Cyclometalated Iridium(III) Complexes, *Inorg. Chem.*, 2005, **44**(13), 4445–4447, DOI: **10.1021/ic050324u**.

9 T. Hofbeck and H. Yersin, The Triplet State of Fac-$Ir(Ppy)_3$, *Inorg. Chem.*, 2010, **49**(20), 9290–9299, DOI: **10.1021/ic100872w**.

10 M. Montalti, A. Credi, L. Prodi and M. T. Gandolfi, *Handbook of Photochemistry*, CRC Press, 3rd edn, 2006, vol. 633.

11 M. Z. Shafikov, A. V. Zaytsev, V. N. Kozhevnikov and R. Czerwieniec, Aligning Π-Extended Π-Deficient Ligands to Afford Submicrosecond Phosphorescence Radiative Decay Time of Mononuclear Ir(III) Complexes, *Inorg. Chem.*, 2023, **62**(2), 810–822, DOI: **10.1021/acs.inorgchem.2c03403**.

12 R. M. Edkins, Y.-T. Hsu, M. A. Fox, D. Yufit, A. Beeby and R. J. Davidson, Divergent Approach for Tris-Heteroleptic Cyclometalated Iridium Complexes Using Triisopropylsilyl-ethynyl-Substituted Synthons, *Organometallics*, 2022, **41**(17), 2487–2493, DOI: **10.1021/acs.organomet.2c00292**.

13 S. Kappaun, C. Slugovc and E. J. W. List, Phosphorescent Organic Light-Emitting Devices: Working Principle and Iridium Based Emitter Materials, *Int. J. Mol. Sci.*, 2008, **9**, 1527–1547.

14 H. Yersin, A. F. Rausch, R. Czerwieniec, T. Hofbeck and T. Fischer, The Triplet State of Organo-Transition Metal Compounds. Triplet Harvesting and Singlet Harvesting for Efficient Oleds, *Coord. Chem. Rev.*, 2011, **255**(21–22), 2622–2652, DOI: **10.1016/j.ccr.2011.01.042**.

15 E. Longhi and L. De Cola, in Iridium(III) Complexes for Oled Application, *Iridium(III) in Optoelectronic and Photonics Applications*, 2017, pp. 205–274.

16 J. Jayabharathi, V. Thanikachalam and S. Thilagavathy, Phosphorescent Organic Light-Emitting Devices: Iridium Based Emitter Materials – an Overview, *Coord. Chem. Rev.*, 2023, **483**, 215100, DOI: **10.1016/j.ccr.2023.215100**.

17 G. Hong, X. Gan, C. Leonhardt, Z. Zhang, J. Seibert, J. M. Busch and S. Bräse, A Brief History of Oleds—Emitter Development and Industry Milestones, *Adv. Mater.*, 2021, **33**(9), 2005630, DOI: **10.1002/adma.202005630**.

18 S. Meksawangwong, B. Gohil, W. Punyain, R. Pal and F. Kielar, Development of Tris-Cyclometalated Iridium Complexes for Cellular Imaging through Structural Modification, *Inorg. Chim. Acta*, 2020, **508**, 119609, DOI: **10.1016/j.ica.2020.119609**.

19 K. K.-W. Lo and K. Y. Zhang, Iridium(III) Complexes as Therapeutic and Bioimaging Reagents for Cellular Applications, *RSC Adv.*, 2012, **2**(32), 12069–12083, DOI: **10.1039/C2RA20967E**.

20 S. Abbas, I.-U.-D. Din, A. Raheel and A. Tameez ud Din, Cyclometalated Iridium (III) Complexes: Recent Advances in Phosphorescence Bioimaging and Sensing Applications, *Appl. Organomet. Chem.*, 2020, **34**(3), e5413, DOI: **10.1002/aoc.5413**.

21 L. C.-C. Lee and K. K.-W. Lo, Shining New Light on Biological Systems: Luminescent Transition Metal Complexes

for Bioimaging and Biosensing Applications, *Chem. Rev.*, 2024, **124**(15), 8825–9014, DOI: 10.1021/acs.chemrev.3c00629.

22 A. Nakagawa, Y. Hisamatsu, S. Moromizato, M. Kohno and S. Aoki, Synthesis and Photochemical Properties of Ph Responsive Tris-Cyclometalated Iridium(III) Complexes That Contain a Pyridine Ring on the 2-Phenylpyridine Ligand, *Inorg. Chem.*, 2014, **53**(1), 409–422, DOI: 10.1021/ic402387b.

23 X.-D. Bi, R. Yang, Y.-C. Zhou, D. Chen, G.-K. Li, Y.-X. Guo, M.-F. Wang, D. Liu and F. Gao, Cyclometalated Iridium(III) Complexes as High-Sensitivity Two-Photon Excited Mitochondria Dyes and near-Infrared Photodynamic Therapy Agents, *Inorg. Chem.*, 2020, **59**(20), 14920–14931, DOI: 10.1021/acs.inorgchem.0c01509.

24 L. Zhang and D. Ding, Recent Advances of Transition Ir(III) Complexes as Photosensitizers for Improved Photodynamic Therapy, *VIEW*, 2021, **2**(6), 20200179, DOI: 10.1002/VIW.20200179.

25 T. M. Monos and C. R. J. Stephenson, Photoredox Catalysis of Iridium(III)-Based Photosensitizers, in *Iridium(III) in Optoelectronic and Photonics Applications*, ed. E. Zysman-Colman, John Wiley and Sons, Ltd., Sussex, England, 2017, pp. 541–581.

26 M. R. Schreier, X. Guo, B. Pfund, Y. Okamoto, T. R. Ward, C. Kerzig and O. S. Wenger, Water-Soluble Tris(Cyclometalated) Iridium(III) Complexes for Aqueous Electron and Energy Transfer Photochemistry, *Acc. Chem. Res.*, 2022, **55**(9), 1290–1300, DOI: 10.1021/acs.accounts.2c00075.

27 I. S. Alkhaibari, X. Zhang, J. Zhao, T. M. Stonelake, R. C. Knighton, P. N. Horton, S. J. Coles, N. J. Buurma, E. Richards and S. J. A. Pope, Tuning Excited State Character in Iridium(III) Photosensitizers and Its Influence on Tta-Uc, *Inorg. Chem.*, 2024, **63**(21), 9931–9940, DOI: 10.1021/acs.inorgchem.4c01003.

28 C. S. K. Mak, D. Pentlehner, M. Stich, O. S. Wolfbeis, W. K. Chan and H. Yersin, Exceptional Oxygen Sensing Capabilities and Triplet State Properties of Ir(Ppy-Nph$_2$)$_3$, *Chem. Mater.*, 2009, **21**(11), 2173–2175, DOI: 10.1021/cm9003678.

29 J. Li, P. I. Djurovich, B. D. Alleyne, M. Yousufuddin, N. N. Ho, J. C. Thomas, J. C. Peters, R. Bau and M. E. Thompson, Synthetic Control of Excited-State Properties in Cyclometalated Ir(III) Complexes Using Ancillary Ligands, *Inorg. Chem.*, 2005, **44**(6), 1713–1727, DOI: 10.1021/ic048599h.

30 K. P. S. Zanoni, B. K. Kariyazaki, A. Ito, M. K. Brennaman, T. J. Meyer and N. Y. Murakami Iha, Blue-Green Iridium(III) Emitter and Comprehensive Photophysical Elucidation of Heteroleptic Cyclometalated Iridium(III) Complexes, *Inorg. Chem.*, 2014, **53**(8), 4089–4099, DOI: 10.1021/ic500070s.

31 K. Dedeian, J. M. Shi, N. Shepherd, E. Forsythe and D. C. Morton, Photophysical and Electrochemical Properties of Heteroleptic Tris-Cyclometalated Iridium(III) Complexes, *Inorg. Chem.*, 2005, **44**(13), 4445–4447.

32 W. Leslie, R. A. Poole, P. R. Murray, L. J. Yellowlees, A. Beeby and J. A. G. Williams, Near Infra-Red Luminescence from Bis-Terpyridyl Iridium(III) Complexes Incorporating Electron-Rich Pendants, *Polyhedron*, 2004, **23**(17), 2769–2777.

33 S. Lamansky, P. Djurovich, D. Murphy, F. Abdel-Razzaq, H.-E. Lee, C. Adachi, P. E. Burrows, S. R. Forrest and M. E. Thompson, Highly Phosphorescent Bis-Cyclometalated Iridium Complexes: Synthesis, Photophysical Characterization, and Use in Organic Light Emitting Diodes, *J. Am. Chem. Soc.*, 2001, **123**(18), 4304–4312, DOI: 10.1021/ja003693s.

34 S. Lamansky, P. Djurovich, D. Murphy, F. Abdel-Razzaq, R. Kwong, I. Tsyba, M. Bortz, B. Mui, R. Bau and M. E. Thompson, Synthesis and Characterization of Phosphorescent Cyclometalated Iridium Complexes, *Inorg. Chem.*, 2001, **40**(7), 1704–1711.

35 T. Sajoto, P. I. Djurovich, A. B. Tamayo, J. Oxgaard, W. A. Goddard and M. E. Thompson, Temperature Dependence of Blue Phosphorescent Cyclometalated Ir(III) Complexes, *J. Am. Chem. Soc.*, 2009, **131**(28), 9813–9822, DOI: 10.1021/ja903317w.

36 R. J. Holmes, S. R. Forrest, Y. J. Tung, R. C. Kwong, J. J. Brown, S. Garon and M. E. Thompson, Blue Organic Electrophosphorescence Using Exothermic Host-Guest Energy Transfer, *Appl. Phys. Lett.*, 2003, **82**(15), 2422–2424, DOI: 10.1063/1.1568146.

37 A. F. Rausch, H. H. H. Homeier and H. Yersin, Organometallic Pt(Ii) and Ir(III) Triplet Emitters for Oled Applications and the Role of Spin-Orbit Coupling: A Study Based on High-Resolution Optical Spectroscopy, *Top. Organomet. Chem.*, 2010, **29**, 193–235, DOI: 10.1007/3418_2009_6.

38 M. Kleinschmidt, C. van Wüllen and C. M. Marian, Intersystem-Crossing and Phosphorescence Rates in Fac-Ir^{iii}(Ppy)$_3$: A Theoretical Study Involving Multi-Reference Configuration Interaction Wavefunctions, *J. Chem. Phys.*, 2015, **142**(9), 094301, DOI: 10.1063/1.4913513.

39 M. Nonoyama, Benzo[H]Quinolin-10-Yl-N Iridium(III) Complexes, *Bull. Chem. Soc. Jpn.*, 1974, **47**(3), 767–768, DOI: 10.1246/bcsj.47.767.

40 A. Suzuki, Synthetic Studies Via the Cross-Coupling Reaction of Organoboron Derivatives with Organic Halides, *Pure Appl. Chem.*, 1991, **63**(3), 419, DOI: 10.1351/pac199163030419.

41 A. Yu. Gitlina, F. Fadaei-Tirani, A. Ruggi, C. Plaice and K. Severin, Acid-Base-Induced Fac → Mer Isomerization of Luminescent Iridium(III) Complexes, *Chem. Sci.*, 2022, **13**(35), 10370–10374, DOI: 10.1039/D2SC02808E.

42 T. Hofbeck and H. Yersin, The Triplet State of Fac-Ir(Ppy)$_3$, *Inorg. Chem.*, 2010, **49**(20), 9290–9299, DOI: 10.1021/ic100872w.

43 S. Lamansky, P. Djurovich, D. Murphy, F. Abdel-Razzaq, R. Kwong, I. Tsyba, M. Bortz, B. Mui, R. Bau and M. E. Thompson, Synthesis and Characterization of Phosphorescent Cyclometalated Iridium Complexes, *Inorg. Chem.*, 2001, **40**(7), 1704–1711, DOI: 10.1021/ic0008969.

44 J. R. Lakowicz, in *Measurement of Fluorescence Lifetimes, Principles of Fluorescence Spectroscopy*, ed. J. R. Lakowicz, Springer US, Boston, MA, 1983, pp. 51–93.

45 Y. Shao, Z. Gan, E. Epifanovsky, A. T. B. Gilbert, M. Wormit and J. Kussmann, *et al.*, Advances in Molecular Quantum Chemistry Contained in the Q-Chem 4 Program Package, *Mol. Phys.*, 2015, **113**(2), 184–215, DOI: **10.1080/00268976.2014.952696**.

46 Y. Zhao and D. G. Truhlar, The M06 Suite of Density Functionals for Main Group Thermochemistry, Thermochemical Kinetics, Noncovalent Interactions, Excited States, and Transition Elements: Two New Functionals and Systematic Testing of Four M06-Class Functionals and 12 Other Functionals, *Theor. Chem. Acc.*, 2008, **120**(1), 215–241, DOI: **10.1007/s00214-007-0310-x**.

47 F. Weigend and R. Ahlrichs, Balanced Basis Sets of Split Valence, Triple Zeta Valence and Quadruple Zeta Valence Quality for H to Rn: Design and Assessment of Accuracy, *Phys. Chem. Chem. Phys.*, 2005, **7**(18), 3297–3305, DOI: **10.1039/b508541a**.

48 D. Bohm and D. Pines, A Collective Description of Electron Interactions. I. Magnetic Interactions, *Phys. Rev.*, 1951, **82**(5), 625–634, DOI: **10.1103/PhysRev.82.625**.

49 D. Pines and D. Bohm, A Collective Description of Electron Interactions: Ii. Collective Vs Individual Particle Aspects of the Interactions, *Phys. Rev.*, 1952, **85**(2), 338–353, DOI: **10.1103/PhysRev.85.338**.

50 D. Bohm and D. Pines, A Collective Description of Electron Interactions: III. Coulomb Interactions in a Degenerate Electron Gas, *Phys. Rev.*, 1953, **92**(3), 609–625, DOI: **10.1103/PhysRev.92.609**.

51 G. J. Hedley, A. Ruseckas and I. D. W. Samuel, Ultrafast Luminescence in $Ir(Ppy)_3$, *Chem. Phys. Lett.*, 2008, **450**(4), 292–296, DOI: **10.1016/j.cplett.2007.11.028**.

52 G. J. Hedley, A. Ruseckas and I. D. W. Samuel, Ultrafast Intersystem Crossing in a Red Phosphorescent Iridium Complex, *J. Phys. Chem. A*, 2009, **113**(1), 2–4, DOI: **10.1021/jp808944n**.

53 M. J. Peach, P. Benfield, T. Helgaker and D. J. Tozer, Excitation Energies in Density Functional Theory: An Evaluation and a Diagnostic Test, *J. Chem. Phys.*, 2008, **128**(4), 044118, DOI: **10.1063/1.2831900**.